

Realistic photonic bandgap structures for TM-polarized light for all-optical switching

Ping Ma, Franck Robin, Heinz Jäckel

Communication Photonics Group, Electronics Laboratory, ETH Zurich, 8092 Zurich, Switzerland

pingma@if.ee.ethz.ch

<http://www.ife.ee.ethz.ch>

Abstract: We investigate manufacturable photonic crystal (PhC) structures with a large photonic bandgap for TM-polarized light. Although such PhC structures have been the object of only a limited number of studies to date, they are of central importance for ultra fast all-optical switches relying on intersubband transitions in AlAsSb/InGaAs quantum wells, which support only TM polarization. In this paper, we numerically study substrate-type PhCs for which the two-dimensional approximation holds and three-dimensional photonic-crystal slabs, both with honeycomb lattice geometry. Large TM PBGs are obtained and optimized for both cases. Two types of PhC waveguides are proposed which are able to guide TM modes. Their unique properties show the potential to apply as waveguiding structures in all-optical switches.

©2006 Optical Society of America

OCIS codes: (999.9999) Photonic crystals; (130.2790) Guided Waves; (230.1150) All-optical devices

References and links

1. S. Kawanishi, "Ultrahigh-speed optical time-division-multiplexed transmission technology based on optical signal processing," *IEEE J. Quantum Electron.* **34**, 2604 (1998).
2. M. Nakazawa, "Tb/s OTDM technology," *Proc. 27 Eur. Conf. on Opt. Commun.* **184** (2001).
3. P. Cristea, Y. Fedoryshyn, and H. Jäckel, "Growth of AlAsSb/InGaAs MBE-layers for all optical switches," *J. Crystal Growth.* **278**, 544-547 (2005).
4. H. Yoshida, T. Mozume, A. Neogi and O. Wada, "Ultrafast all-optical switching at 1.3 μ m/1.55 μ m using novel InGaAs/AlAsSb/InP coupled double quantum well structure for intersubband transitions," *Electron. Lett.* **35**, 1103 (1999).
5. A V Petrov and M. Eich, "Zero dispersion at small group velocities in photonic crystal waveguides," *Appl. Phys. Lett.* **85**, 4866-4868 (2004).
6. T. Tanabe, M. Notomi, S. Mitsugi, A. Shinya and E. Kuramochi, "All-optical switches on a silicon chip realized using photonic crystal nanocavities," *Appl. Phys. Lett.* **87**, 151112 (2005).
7. J. D. Joannopoulos, R. D. Meade, J. N. Winn, *Photonic Crystal: Molding the Flow of Light* (Princeton University Press, Princeton, NJ, 1995).
8. S. G. Johnson, S. Fan, P. R. Villeneuve, J. D. Joannopoulos and L. A. Kolodziejski, "Guided modes in photonic crystal slabs," *Phys. Rev. B* **60**, 5751 (1999).
9. W C L. Hopman, R M de Ridder, C. G. Bostan, S. Selvaraja, V. J. Gadgil, L. Kuipers and A. Driessen, "Design and Fabrication of 2-Dimensional Silicon Photonic Crystal Membranes by Focused Ion Beam Processing," presented at the ePiXnet winterschool on Optoelectronic Integration: Technology and Applications, ePiXnet Winter School, Pontresina, Switzerland, 13-17 Mar. 2006.
10. G. Stark, R. Wüest, F. Robin, D. Erni, H. Jäckel, A. Christ, N. Kuster, "Extraction of the geometric parameters of photonics crystals using the effective-index method," submitted to *Opt. Lett.*
11. P. R. Villeneuve and M. Piché, "Photonic band gaps in two-dimensional square and hexagonal lattices," *Phys. Rev. B* **46**, 4969 (1992).
12. D. Cassagne, C. Jouanin and D. Bertho, "Hexagonal photonic-band-gap structures," *Phys. Rev. B* **53**, 7134 (1996).
13. S. Rowson, A. Chelnokov, J. M. Lourtioz and F. Carcenac, "Reflection and transmission characterization of a hexagonal photonic crystal in the mid infrared," *J. Appl. Phys.* **83**, 5061-5064 (1998).
14. J. Ye, V. Mizeikis, Y. Xu, S. Matsuo and H. Misawa, "Fabrication and optical characteristics of silicon-based two-dimensional photonic crystals with honeycomb lattice," *Opt. Commun.* **211**, 205-213 (2002).
15. S. G. Johnson and J. D. Joannopoulos, "Block-iterative frequency-domain methods for Maxwell's equations in a planewave basis," *Opt. Express* **8** 173-190 (2001).

16. M. Kafesaki, C. M. Soukoulis and M. Agio, "Losses and transmission in two-dimensional slab photonic crystals," *Appl. Phys.* **96**, 4033-4038 (2004).
17. C. G. Bostan and R. M. de Ridder, "Design of photonic crystal slab structures with absolute gaps in guided modes," *J. Optoelectron. Adv Mater.* **4**, 921-928 (2002).
18. C. Y. Kao, S. Osher, and E. Yablonovitch, "Maximizing band gaps in two-dimensional photonic crystals by using level set methods," *Appl. Phys. B* **81**, 235-244 (2005).
19. Y. Sugimoto, N. Ikeda, N. Carlsson, K. Asakawa, N. Kawai and K. Inoue, "Fabrication and characterization of different types of two-dimensional AlGaAs photonic crystal slabs," *J. Appl. Phys.* **91**, 922-929 (2002).
20. A. Yariv and P. Yeh, *Optical Waves in Crystals* (Wiley, New York, 1984).
21. M. Qiu, "Band gap effects in asymmetric photonic crystal slabs," *Phys. Rev. B* **66**, 033103 (2002).
22. M. Qiu, "Effective index method for heterostructures-slab-waveguide-based two-dimensional photonic crystals" *Appl. Phys. Lett.* **81**, 1163-1165 (2002).
23. S. G. Johnson, P. R. Villeneuve, S. Fan, and J. D. Joannopoulos, "Linear waveguides in photonic-crystal slabs," *Phys. Rev. B* **62**, 8212 (2000).
24. Y. Tanaka, Y. Sugimoto, N. Ikeda, H. Nakamura, Y. Watanabe, K. Asakawa and K. Inoue, "Guided modes of a width-reduced photonic-crystal slab line-defect waveguide with asymmetric cladding," *J. Lightwave Technol.* **23**, 2749-2755 (2005).
25. A. V. Gopal, H. Yoshida, T. Simoyama, N. Georgiev, T. Mozume and H. Ishikawa, "Understanding the ultra-low intersubband saturation intensity in InGaAs-AlAsSb quantum wells," *IEEE J. Quantum Electron.* **39**, 299-305 (2003).

1. Introduction

All-optical telecommunication networks with transmission rates in the Tbit/s range will be needed to fulfill the demands posed by the rapid growth of the Internet traffic [1]. Such networks can be constructed from Optical Time-Division-Multiplex / Wavelength-Division-Multiplex (OTDM/WDM) (or mixed) systems, and ultrafast semiconductor-based all-optical devices are one of the key technologies for such systems [2]. Nonlinear optical devices that are able to switch ultrafast optical pulses (<1ps) at low optical pulse energy (<100 fJ/ μm^2) are required. Switches relying on intersubband transitions (ISBT) within the conduction band exhibit ultrafast relaxation time and large optical nonlinearities. Transitions in the telecommunication wavelength range are achievable, e.g., in InGaAs/AlAsSb quantum wells (QWs) exhibiting a large conduction band discontinuity of 1.6 eV [3, 4].

The combination of efficient transmission and strong localization is important for all-optical switching. For practical devices, a reduction of the switching energy below 100fJ has to be achieved. Photonic crystals (PhCs) are promising candidates as waveguiding structures for all-optical switches. Indeed, the nonlinear light-matter interactions and the photon density can be increased in the active region by a high transverse optical confinement and a decrease of the light group velocity in photonic crystal waveguides (PhCWs) [5] or/and by introducing PhC cavities [6], which are unique features compared to their photonic-wire counterparts relying solely on index guiding.

On the other hand, intersubband transitions are strongly polarization-dependent and it is therefore necessary to search for large transverse-magnetic (TM) photonic bandgaps (PBGs). Until now, little attention has been devoted to PhC structures for TM polarization, since only a narrow PBG is available for this polarization in the conventionally studied PhCs with a triangular lattice of air holes. As an alternative, it is well-known that large TM PBGs can be supported by isolated dielectric rods [7] [8]. However, coupling guided modes back to the active core layers after propagating through air gaps is challenging, because the out-of-plane energy loss is expected to be high. Additionally, such structures are likely to suffer from a lack of mechanical stability. A possible solution would be the utilization of background filling materials [9]. For the PhCs of practical interest with air holes etched in a dielectric material, PhCs relying on the honeycomb lattice geometry exhibit the largest TM PBG compared to the PhCs based on triangular and square lattice geometries. Photonic crystal slabs, which confine the optical fields in the vertical direction by the refractive index guiding mechanism, is a more easily fabricated alternative to a true three-dimensional (3D) periodic PhC structure. In this paper, we theoretically investigate PhC structures with honeycomb geometry exhibiting large TM-polarized PBGs, using both two-dimensional numerical simulations aiming for low vertical index contrast PhC slabs (e.g., InP-based substrate type) and full three-dimensional

simulations mandatory for air-bridge (membrane) type PhC slabs. The proposed PhCWs are capable to guide TM-modes that are required for all-optical switches. The desired wavelengths for the control and signal pulses should be centered around 1300nm or 1550nm for optimum use of the transparency windows of optical fibers. An ideal waveguide design would present one mode at each wavelength to match optical phonon resonances. Alternative designs would rely on two closely-spaced wavelengths using the same ISBT. Due to the limitations of our optical characterization setup, we focus this paper on the 1550nm and/or 1760nm bands.

2. Photonic crystals with the honeycomb lattice geometry

2.1 Two-dimensional (2D) simulations of substrate-type PhCs

For low-vertical-index-contrast systems such as substrate-type InGaAsP/InP PhC slabs, 2D simulations show a high degree of accuracy, both compared to the realistic but time-consuming 3D simulations and the experimental extractions of PhCWs dispersion relations [10]. To date, 2D studies of PhCs with honeycomb lattice geometry have been performed both theoretically [11, 12] and experimentally [13, 14]. A definition of the honeycomb lattice geometry is shown in Fig. 1. This lattice can be viewed as the superposition of two triangular sublattices, with the unit cell containing two air holes. The reciprocal lattice vectors and the irreducible Brillouin zone remain the same as those of the triangular lattice. The average refractive index of the high dielectric material we used in this paper for the 2D simulations is 3.24 and corresponds to periodic stacks of InGaAs/AlAsSb quantum wells exhibiting ISBTs [4].

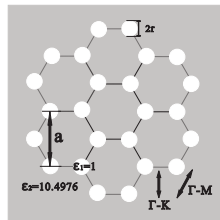


Table 1. TM PBG Comparison

Lattice geometry	TM-PBG size	r/a
Triangular	3.9%	0.43
Square	7%	0.43
Honeycomb	11% and 8%	0.24

Fig. 1. Definition of honeycomb PhC lattice and comparison of maximum relative TM PBG width for triangular, square and honeycomb lattices.

The band structures are simulated with the freely available software package MPB that implements an iterative eigensolver of Maxwell's equations on a planar wave basis [15]. The maximum normalized TM PBG widths of three different lattices of air holes are summarized in Table I. Taking the fabrication limitations into account, only moderate air-filling factor PhCs are considered with $r < 0.43a$ for triangular and square lattices, where a is the lattice constant. For the honeycomb lattice geometry, attention should be paid to avoid an overlapping of nearest neighboring elements (the close-packed configuration). The holes-radii upper limit is $0.5a/(3^{1/2}) \approx 0.288a$, which corresponds to a maximum air-filling factor of approximately 60%, compared to over 90% for the close-packed configuration in the triangular lattice. A relatively low filling factor nevertheless yielding a large PBG shows twofold benefits: (i) it gives a large volume of high dielectric material, thus increasing the light-matter interactions and (ii) decreases the propagation losses which are roughly proportional to the filling factor [16]. The honeycomb PhCs with manufacturable hole radii of $r=0.24a$ exhibits the largest TM PBG. The maximum mid-gap ratio is 11.1% and 8% for the first and second gaps, respectively, with center frequencies of 0.231 and 0.423 in normalized frequency ($\omega a/2\pi c$), as shown in Fig. 2(a). This large TM PBG can be explained by the circular Brillouin zone of the honeycomb geometry. Indeed, we found a circular confinement (shape of the holes) to be beneficial for a large TM PBG, because it matches the shape of

Brillouin zone [17]. Additionally, the remaining materials around the air holes isolate the high dielectric regions more efficiently than the square and triangular lattices.

Furthermore, although a few more complex structures can be modeled to achieve TM PBG by varying additional parameters, e.g., the lattice type, the shape of the air holes etc., most of them show limited manufacturability at telecommunication wavelengths. For instance, Kao *et.al.*, [18] used optimization algorithms to maximize the PBG, resulting in complicated patterns but it is very questionable whether such shapes could be fabricated accurately in the nanometer range.

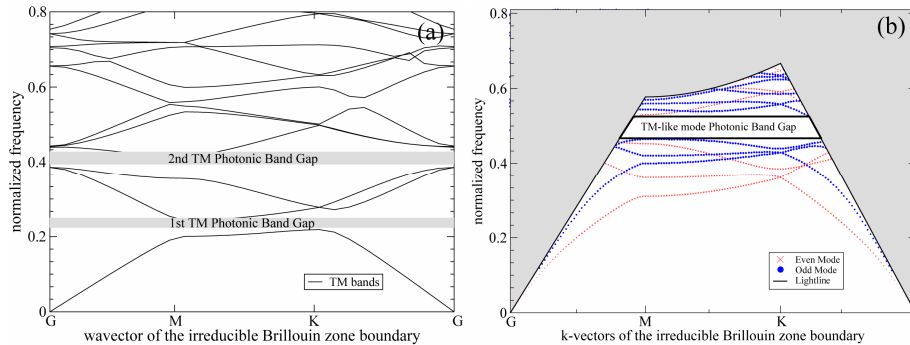


Fig. 2. Band diagram of honeycomb-type PhCs with $r=0.24a$. (a) Two-dimensional simulation, (b) Full three-dimensional simulation of air-bridge type PhC slab with thickness $0.45a$, projected band diagram.

2.2 Three-dimensional (3D) simulations for air-bridge type PhC slabs

The air-bridge type PhC membrane, which consists of a PhC structure etched through a thin (ca. 240nm) membrane suspended in air, is superior to the conventional substrate-type PhC slab structure for low propagation loss [19], because of its stronger vertical mode confinement that attenuates the guided-modes coupling into radiation modes. Low loss is crucial for a low switching-energy device. Nevertheless, if the core layer of the optical structure is thin (and comparable to the wavelength) and the index contrast in the vertical direction is strong, full three-dimensional simulations become compulsory. Figure 2(b) shows the 3D simulation result of an air-bridge type PhC membrane with honeycomb lattice geometry, and holes of radius $0.24a$. For guided modes in the communication wavelength range, a slab thickness less than 340nm is required to maintain a single-mode operation with an approximate weighed average refractive index of air and dielectric material of the core layer [20]. The modes above the light-cone are not considered because unlike the Bloch guided modes, they should exponentially decay into the cladding layers. Therefore, although radiation modes are available within the frequency range of the PBG, no mode can be guided in the plane of the slab above the light cone. Due to the symmetry of our slab structure, the modes can be categorized into even and odd modes, according to their symmetries to the plane bisecting the slab. No mode mixing is possible in principle. Since only fundamental modes well exist in the PhC slab, the even modes are TE_0 -like and odd modes are TM_0 -like with respect to the mirror plane [21]. The photonic band diagram for the parameters given above is shown in Fig. 2(b). The gap is from 0.458 to 0.525, which gives a mid-gap ratio of 14%. This complete gap is large enough to cover the communication wavelength range from 1450nm to 1660nm using a lattice constant of 760nm.

Comparing the 2D and 3D band diagrams, we observe an obvious blue shift of the TM modes, especially for bands at lower frequencies, but they more or less maintain their orders and shapes. Thus the first TM PBG between the first and second bands disappears, while the second PBG between the third and fourth bands remains but at a higher frequencies range. In such high-index-contrast heterostructures, the effective index method for 2D simulation is found not to be valid for such a wide frequency region.

To achieve a large TM PBG a large filling factor, requiring a narrow spacing between holes, is necessary and thus high fabrication accuracy in terms of r/a reproducibility is needed. In practice, using a hole radius $r=0.24a$, for a lattice constant of 760nm the separation between holes is larger than 70nm, which is easily manufacturable using electron-beam lithography. It is also relevant to discuss the impact of the fabrication tolerance of the hole radius on the size and spectral position of the PBG. A good monitor of this influence can be obtained from the gap map diagram as shown in Fig. 3(a), which maps the dielectric- and air-band edge frequencies of PBGs as a function of the r/a ratio. For the bands in the high-frequency region, the energy locates mainly in the high dielectric region, so these should be highly sensitive on the filling factor. This is confirmed by the large frequency shift of the high-frequency air-band edge compared to the low-frequency dielectric-band edge. By reducing the hole radius to $0.23a$, the gap covers the reduced frequency range from 0.452 to 0.509, yielding a mid-gap ratio of 11.9%, while the air and dielectric bands are shifted by 3% and 1%, respectively.

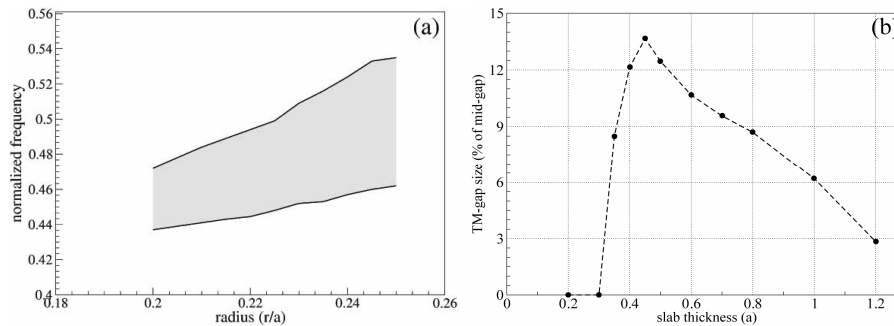


Fig. 3. Three-dimensional simulation of TM PBG in air membrane. (a) TM gap map, (b) Gap size (normalized to mid-gap frequency) versus slab thickness.

The influence of the slab thickness on the gap size is also investigated. The mid-gap width vs. slab thickness is shown in Fig. 3(b). For a thick slab, the higher-order modes will be more easily excited by adding horizontal nodal planes. Such modes may lie slightly above the lower-order modes, preventing any PBG formation. For a thin slab, only a weak perturbation of the background dielectric material will occur. Thus, the few guided modes existing in the slab remain closer to the light cone and are weakly guided due to the high losses [8]. The optimal thickness from simulations is $0.45a$. Additionally, the simulations show that the dielectric- and air-band edges shift towards lower frequencies for an increasing slab thickness. This behavior can be explained by the fact that the fraction of the optical mode propagating through the dielectric material is larger for thicker slabs, thus shifting the photonic bandgap in a similar fashion as a reduction of the filling factor.

3. Waveguide designs in honeycomb lattice geometry

In order to create PhCWs, we break the periodicity of the PhCs in one direction and thus introduce linear defects, creating localized bands that fall within and are confined by the PBG. Since the wave vector region for waveguides in the Γ - M direction is shorter than in the Γ - K direction, the PBGs are likely to locate above the cladding light line. We propose two types of line defect PhCWs in the Γ - K direction based on the honeycomb lattice geometry: the missing-hole waveguide formed by removing two rows of holes for a symmetric design as depicted in Fig. 4(a) and the additional-hole waveguide formed by introducing one row of holes in the center of the honeycomb lattice as illustrated in Fig. 4(b).

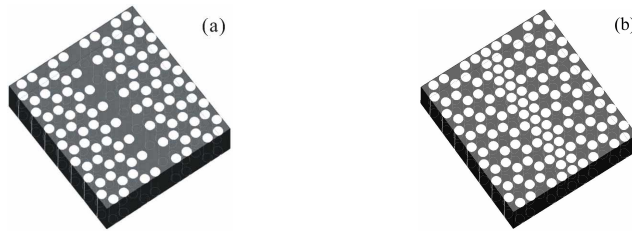


Fig. 4. Schematic representation of the designed linear-defect PhCWs. (a) Missing-hole waveguide, created by removing two rows of holes in the Γ -K direction. (b) Additional-hole waveguide, created by adding one row of holes with the same radii in the Γ -K direction.

We first simulate the waveguide designs using two-dimensional simulations, which provide valuable first insights into the physics of the PhCWs, especially in the view of the computational cost of full 3D simulations. Together with the effective index approximation, it is found that 2D simulations are accurate enough to replace 3D simulations also for waveguides as long as the low-index-contrast heterostructures slab waveguide is single mode for the frequency region of interest [22]. The dispersion relations of the PhCWs are shown in Fig. 5(a) and 6(a) for the missing- and additional-hole PhCWs, respectively. Defining the waves propagation in the y direction, a TM mode has the components H_x , E_y , and E_z . In two dimensions, the waveguide modes can also be classified as laterally even or odd parities according to the symmetry of the E_z component with respect to the plane bisecting the waveguide. Based on the definition above, relying on the mode profiles shown in the Fig. 5(b), we identified the guided modes parities from the different bands with respect to the parity of the E_z field. Dispersion curves of the modes with opposite parity can cross, regardless of the mode order, while the ones of modes with identical parities and different orders repel each other, giving rise to so-called mini-stopbands. 3D FDTD simulations can be used to determine how efficiently each propagating mode couple from access waveguides into the PhCWs, considering its modal and impedance mismatch, which is beyond the scope of this paper.

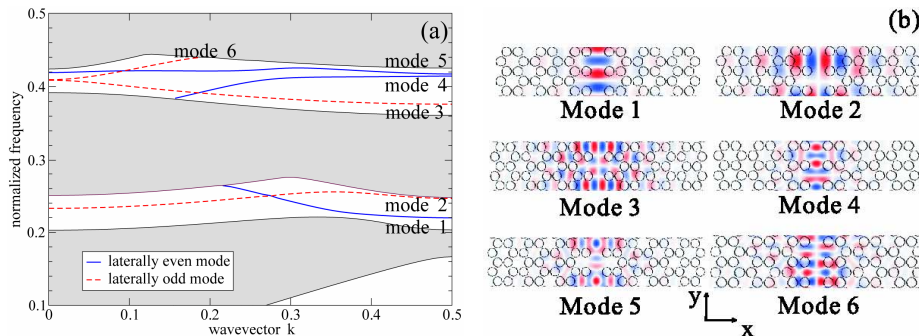


Fig. 5. (a). Two-dimensional computation of the dispersion relation of missing-hole PhCWs in the Γ -K direction, (b). Horizontal E_z field cross-section of the guided modes.

For missing-hole PhCWs, there are one guided mode in the first gap and two guided modes in the second gap both for laterally even and odd modes as shown in Fig. 5(a). Since for each parity there is no overlap of the guided modes in frequency, we consider the PhCW to be quasi-mono-mode over the full wavelength range. The projected band structure for line defects retains a wave-vector quantum number, which means that the range of frequencies available for guided modes may be larger than the range of the projected PBG. One should however keep in mind that this quantum number disappears at locations that break translational symmetry such as at waveguide bends [23], which reduce the available bandwidth compared to the waveguides. A flat slope of the dispersion curve corresponds to a guided mode with a small group velocity, which can be achieved at the Brillouin zone edge. It

is also noteworthy that in the second gap, for each modal parity, a pair of degenerate modes with the same wave vector but opposite group velocities is available. This pair of dispersion curves could potentially be very useful to minimize group-velocity dispersion (GVD). Due to the large width of this waveguide and the cavity-like structure of the honeycomb lattice, the guided modes extend into the PhC claddings. The possible remedy can be either to reduce the waveguide width to, e.g., $W1.5$ or remove two more neighboring rows of holes, and then shift the lattice on both side of the waveguide towards each other [24].

The additional-hole PhCWs also support TM guided modes are shown in Fig. 6(a). There is one laterally even mode inside the first gap and one pair of modes inside the second gap. Since, due to the additional hole, the effective index is lower in the waveguide than in the surrounding sides, the modes are guided horizontally only by PBG confinement. Figure 6(b) shows the influence of changing the additional-hole radius on the guided modes. With larger additional-hole radii, all the guided bands shift upwards. This additional row of holes gives an extra degree of freedom for the design of more complex devices. For example, by changing the radius of one hole in the linear defect, one can make an inline PhC cavity which is useful to increase the light-matter interaction in the switches. As the polarization separation of the signal and control pulses is not possible in AOS devices due to the TM-polarized nature of the ISBTs, one can discriminate them by combining two waveguides with different additional-hole radii.

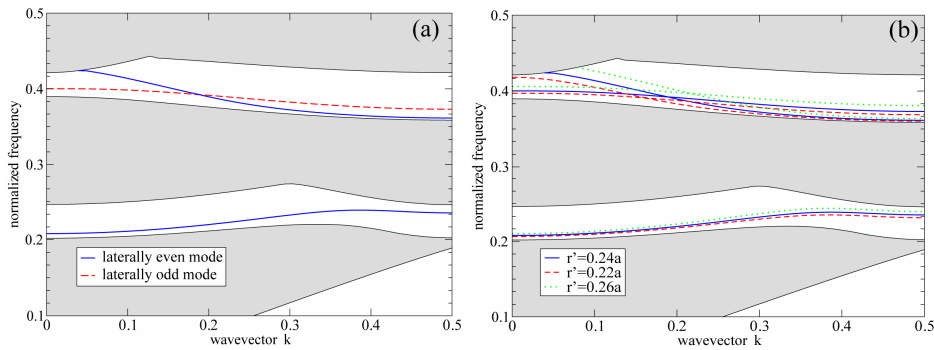


Fig. 6. (a). Two-dimensional computation of the dispersion relation of additional-hole PhCWs in the Γ -K direction. (b). Guided modes for various defect hole radii (bulk radius $0.24a$).

In conclusion regarding the 2D modeling of the waveguide designs, both waveguide types can support TM-modes in each TM PBG. The bandwidth of the guided bands inside the first TM PBG is large enough to support both 1550nm and 1760nm pulses. For example, for a lattice constant of 365nm in low-vertical-index contrast waveguiding structures, the frequency range covered by the even mode in Fig. 6 (a) is from 1535nm to 1775nm. However, the shape of the dispersion curve for this mode makes it only possible to define two closely-spaced wavelengths, e.g., 1500nm and 1560nm, which fulfill the requirements for identical group velocity and minimal GVD for pulse synchronization in a $20\mu\text{m}$ -long waveguide with sub-ps pulse broadening. The associated small lattice constant of 365nm makes it however challenging to manufacture these structures. Additionally, instead of relying on ISBTs for both signal and control pulses, all-optical switches can be envisioned that are based on ISBT-controlled (pump pulse at $1.68\mu\text{m}$, TM-polarization dependent) inter-band transitions (probe pulse at ~ 1.0 - $1.1\mu\text{m}$, polarization-independent)[25]. For this type of switch, one can use guided modes in the lower and upper PBGs simultaneously.

For high-index-contrast air-bridge type PhCWs, we ran 3D simulations for both waveguide designs. Only modes that fall outside both the light cone and the slab bands are truly guided in the line defect, decaying exponentially away from the line defect. In a projected band structure, the new edge of the Brillouin zone is K' instead of K , which is the projected image of the M point onto the Γ -K direction. It is therefore important to consider a

PBG having the air-band edge lower than 0.5 in normalized frequency, which is the intercept of the air line at the K' point to obtain truly guided modes. For this reason and as discussed above, we increased the slab thickness to $0.58a$, which has a TM PBG from 0.415 to 0.462, corresponding to a mid-gap ratio of approximately 11%.

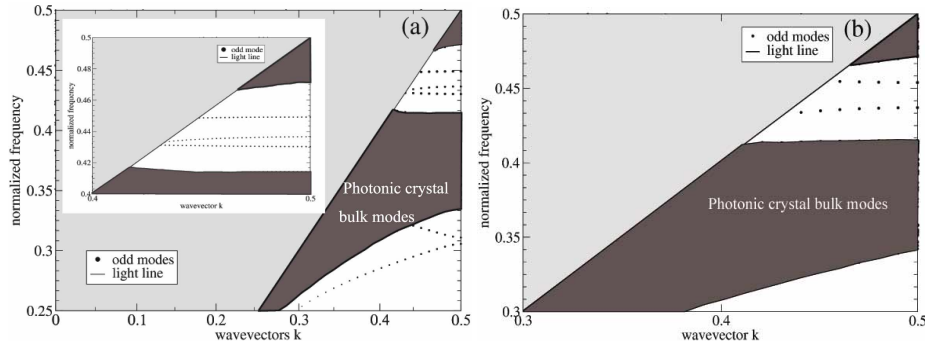


Fig. 7. Three-dimensional simulation of projected band structures of air membrane slab PhCWs in the Γ - K direction, showing the odd-symmetry modes. (a) Missing-hole PhCW (inset: magnified view of gap region) (b) Additional-hole linear defect.

The band diagrams of two waveguide designs are shown in Fig. 7. One can clearly see several flat guided odd modes in the PBGs for both cases. Similar to the 2D simulations, the missing-hole type PhCWs has more guided mode than the additional-hole one, because the increase-index modes drop down from the upper slab bands that has a higher density of states [23]. Since the bands locate at higher frequencies compared to substrate-type PhCWs (2D simulations), the relative bandwidth is not sufficient to cover both 1550nm and 1760nm wavelengths simultaneously. However, one can envisage two solutions. (i) For instance the additional-hole PhCWs can be utilized for propagating two wavelengths at 1550nm and 1610nm relying on the same ISBT as such transitions are usually rather broadband with a 250nm full-width at half-maximum [26]. (ii) Each single pulse can be propagated in separate waveguides by varying the lattice constants. With certain switching-topologies, e.g., a cross-waveguide geometry, one can achieve the switching functionality. As shown in Fig. 7, the flat bands reveal the low group velocity and low GVD properties which are helpful to increase the nonlinear optical interaction in all-optical switches. A compromise has however to be found to achieve low group velocity and large bandwidth simultaneously, for all-optical switches, a 0.5%~1% bandwidth at 1550nm is necessary to propagate a 1ps transform-limited Gaussian pulse. For both waveguide types, the largest bandwidth of a single guided band extracted from the 3D simulations is around 0.8%, which fulfills the requirements.

4. Conclusion

In this paper, we have presented PhC structure designs in the honeycomb lattice geometry to achieve TM PBGs, both for pure two-dimensional PhCs applicable to substrate-type devices and for PhC slabs of air-bridge type membranes. The simulation results show two TM PBGs to be available for the low-index-contrast system while one large TM PBG is present for the high-index-contrast system. Additionally, the two major influencing factors—air-filling ratio and slab thickness—on the size and position of PBGs for air-bridge type PhC membranes are analyzed and optimized.

In a second step, two kinds of PhCWs based on honeycomb lattice geometry are proposed and theoretically studied. Due to strong GVD, investigated waveguides cannot accommodate ISBTs at 1500nm and 1760nm simultaneously. However, the TM-polarized guided modes supported in the low-index-contrast system are applicable directly in all-optical switches relying on two closely-spaced wavelengths at, e.g., 1500nm and 1560nm using the same ISBT. This design guarantees sup-ps pulse broadening for 20 μ m-long waveguides. Concerning the

high-index-contrast system, modes with low group velocity and narrow bandwidth are supported, but the bandwidth is shown to be sufficient for sub-ps range light pulse. The waveguides and more complex designs based on honeycomb type PhCs can be proposed and applied to ISBT all-optical switches.

Acknowledgment

This work is supported by the ETH research grant TH-19/04-3. The authors appreciate useful discussions with Dr. Daniel Erni, Rik Harbers and Katharina Rauscher.